Simultaneous measurements of axial motion and azimuthal rotation of non-uniformities ("spokes") in a Hall thruster

A. Guglielmi, F. Gaboriau, J. Boeuf

▶ **To cite this version:**

A. Guglielmi, F. Gaboriau, J. Boeuf. Simultaneous measurements of axial motion and azimuthal rotation of non-uniformities ("spokes") in a Hall thruster. Physics of Plasmas, 2022, 29 (11), 10.1063/5.0111975 . hal-04262669

HAL Id: hal-04262669
https://hal.science/hal-04262669v1

Submitted on 27 Oct 2023

HAL is a multi-disciplinary open access archive for the deposit and dissemination of scientific research documents, whether they are published or not. The documents may come from teaching and research institutions in France or abroad, or from public or private research centers.

L'archive ouverte pluridisciplinaire **HAL**, est destinée au dépôt et à la diffusion de documents scientifiques de niveau recherche, publiés ou non, émanant des établissements d'enseignement et de recherche français ou étrangers, des laboratoires publics ou privés.

Simultaneous measurements of axial motion and azimuthal rotation of non-uniformities ("spokes") in a Hall thruster

A. Guglielmi, F. Gaboriau,[a] and J.P. Boeuf
LAPLACE, Université de Toulouse, CNRS, INPT, UPS, 118 route de Narbonne, 31062 Toulouse, France

(Dated: September 20, 2022)

Low frequency instabilities are often present in Hall thrusters and are associated with axial and/or azimuthal oscillations of plasma non-uniformities. The axial oscillations are related to the so-called "breathing mode" (periodic depletion of the neutral atom density due to ionization) and are associated with large amplitude current oscillations. The low frequency azimuthal instabilities are characterized by local non-uniformities of the light emission rotating in the azimuthal direction and are generally called "rotating spokes". The possibility of co-existence of these two modes has been discussed in the litterature but without clear experimental evidence of their correlation. In this paper, we present for the first time simultaneous measurements of the axial and azimuthal positions of the spoke. These measurements have been obtained with a high-speed camera using a triangulation method based on parallax. This method has proven to be sufficiently sensitive to track the 3D position (r-θ-z) of local non-uniformities of the light emission. The optical method has been synchronized with measurements of the current on a segmented anode. The results show that under some conditions, breathing oscillations and spoke rotation in the $\mathbf{E}\times\mathbf{B}$ direction are coupled. During the current rise, the spoke moves from the anode region toward the channel exhaust region while rotating in the $\mathbf{E}\times\mathbf{B}$ and seems to follow the movement of the front of neutral atoms progressively filling the channel. About 60 ± 20 % of the total anode current is carried by the spoke.

I. INTRODUCTION

In a Hall thruster the plasma is formed in a channel between two concentric ceramic cylinders.[1] Xenon is injected from the anode side at one end of the channel and is ionized by electrons emitted from an external hot cathode and accelerated by a dc voltage between cathode and anode. A radial magnetic field $\mathbf{B}$ transverse to the applied electric field, with a maximum in the channel exhaust region lowers the axial electron conductivity, leading to an increase of the axial electric field $\mathbf{E}$ in that region. Ions generated in the channel are weakly affected by the magnetic field and are accelerated through the exhaust plane by the axial electric field. The electrons emitted by the external cathode are accelerated by this electric field and ionize the gas injected from the anode upstream of the acceleration region. The residence time of the electrons in the plasma is considerably increased by the radial magnetic field allowing efficient ionization at low gas pressure.

The combination of the radial magnetic field and the axial electric field in the exhaust region leads to a large $\mathbf{E}\times\mathbf{B}$ electron drift and a large azimuthal electron current, the Hall current. Since ions are practically not magnetized (the ion Larmor radius is on the same order of magnitude than the dimension of the thruster channel), the large difference between electron and ion azimuthal drift velocities can lead to charge separation and to the development of instabilities. Moreover, ions cross the acceleration region before they can significantly rotate in the azimuthal direction. Various instabilities, with frequencies ranging from kHz to tens of MHz, and wavelengths from a fraction of mm to several cms, including axial and azimuthal modes, can be present in Hall thrusters. Because instabilities control electron transport across the magnetic field, many experimental and theoretical works have been devoted to the characterization of these instabilities[2]. However, the physics of the instabilities is complex and even though the mechanisms of some of these instabilities have been clarified, their consequences on anomalous electron transport is difficult to quantify and a comprehensive description of the physical phenomena at play is still out of reach. As a result Hall thrusters are generally designed in an empirical manner. Quantifying and controlling electron cross-field mobility in Hall thrusters is essential because the efficiency of Hall thrusters decreases with increasing electron current entering the channel.[3,4].

Among the various instabilities present in Hall thrusters, large amplitude and low frequency oscillations have been known and studied since the earliest ages of Hall thruster development[5,6] and are still the subject of a number of publications. The low frequency intabilities develop along the thruster axis and/or in the azimuthal direction and typically occur in the 5-50 kHz frequency range. The axial mode[7], also called "breathing mode" has been identified as an ionization instability. These axial oscillations strongly depend on the configuration and the intensity of the magnetic field[8] and can be violent or unstable causing the discharge to extinguish. The breathing mode is due to a periodic depletion of neutral atoms in the channel due to ionization, followed by refill of the channel by the neutral flow of atoms injected on the anode side[9]. It can be easily observed through the periodic oscillations of the discharge current and of the light emission. The axial oscillations associated with the breathing mode can be qualitatively described by a 0D predator-prey model[10,11] (Lotka-Volterra equations) but they remain difficult to predict with simulation tools since the mechanisms controlling the instability are quite intricate.[12–17]

The azimuthal rotating mode propagates in the $\mathbf{E}\times\mathbf{B}$ di-

[a]Electronic mail: gaboriau@laplace.univ-tlse.fr

rection at a frequency of a few kHz to a few tens of kHz and is observed as local variations of the potential and of the light emission in the azimuthal direction of the channel thruster.[18–21]. These rotating structures consist of slowly rotating plasma density non-uniformities on which higher frequency fluctuations may be superimposed that also contribute to the so-called anomalous transport.[6,19,22]. Different types of azimuthal instabilities are present in different regions of a Hall thruster. In the region outside the channel, where the magnetic field strength increases in the direction of the exhaust plane, simulations[12,23–25] and experiments[26] have evidenced the presence of an Electron Cyclotron Drift Instability (ECDI). The ECDI is a short wavelength instability (wavelength in the mm range) that leads to collisionless electron transport in the region between cathode and exhaust plane. Since the gas density is very low in this region (and because of its small wavelength) this instability is not associated with visible non-uniformity in the light emission. Instabilities giving rise to azimuthal non-uniformities in the the light emission are more likely to develop in region between the exhaust plane and the anode. In this region the radial magnetic field is large (and decreasing from exhaust plane to anode) and the electric field and plasma density gradients tend to be in the same direction. These conditions are known to be favorable to the development of instabilities (e.g. Simon-Hoh instability[27]). Similar conditions exist in magnetron discharges where rotating spokes are present and have been thoroughly studied experimentally[28,29]. The rotating spokes in magnetron discharges has been clearly identified as a region of strong electron heating and enhanced ionization than can rotate in the $+E \times \mathbf{B}$ or $-E \times \mathbf{B}$ direction depending on the conditions. The rotating spoke of magnetron discharges is therefore an azimuthal ionization wave. Space and time resolved measurement of the plasma potential have shown the presence of a double layer structure at the leading edge of the ionization zone[28]. Results of recent particle-in-cell simulations obtained in simplified conditions are consitent with the experimental observations[30,31]. The question of whether the rotating spokes of Hall thrusters are of the same nature as those observed in magnetron discharges remains to be discussed.

The breathing mode in Hall thrusters is observed at intermediate and high applied voltages for operating conditions where ionization of the gas is very efficient. In most of the studies at intermediate voltages, the azimuthal rotating mode is observed with the breathing mode, e.g. both azimuthal and axial structures coexist[18,32,33]. Furthermore, the capability of controlling the instabilities by modulating externally the applied voltage suggests that there is a coupling between azimuthal and axial modes[33]. A simple explanation of the correlation between the axial breathing mode and the azimuthal rotating mode could be that, under some conditions, the ionization of the neutral front takes place in a helicoidal way i.e. the rotating structure follows the axial displacement toward the anode of the neutral atom front subject to strong ionization. However, to our knowledge, there is no work on the determination of the axial location of the rotating structures nor on the dynamics of the rotating spoke during the breathing mode. The present study aims at determining this issue by using an optical triangulation method (high-speed camera) the axial location of the rotating structure during a period of the breathing mode. A more usual technique using a segmented anode is synchronized with the high-speed camera and allows following the rotating spoke path and estimating the current driven by the spoke itself.

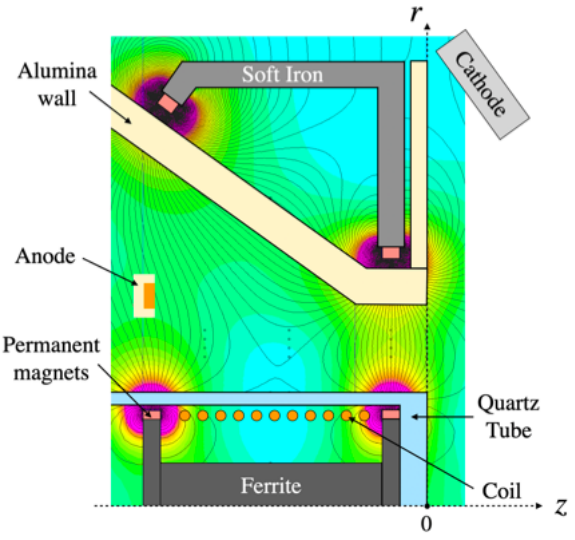

Figure 1. Schematic of the experimental prototype of ID-Hall showing the magnetic field lines. The origin of the axis is fixed in the outer plane on the central axis.

II. EXPERIMENTAL STE-UP AND DIAGNOSTICS

A. ID-Hall thruster

The measurements reported in this article have been performed on a double-stage Hall thruster, ID-Hall (Inductively Double stage Hall thruster), operating in a single-stage mode. The ID-Hall thruster has been developed and tested at the LAPLACE laboratory and its design and properties are described in detail in previous publications[34–36]. Fig. 1 shows a schematic view of the ID-Hall prototype. The axis origin is set at the intersection between the thruster axis and the exhaust plane. The characteristic feature of ID-Hall is that the ionization stage is composed of a magnetized inductive RF plasma source placed inside the central cylinder. The external wall is made of alumina and has two distinct regions: a cylindrical channel of 46 mm in diameter and 10 mm in length and a conical-shaped wall that extends from the channel diameter to a 92 mm diameter in a length of 30 mm. The volume of the ionization chamber is increased (conical shape of the external wall) in order to limit ion losses on the walls, before acceleration and extraction of ions. The inductive plasma source is contained inside a 26 mm diameter Quartz tube that also acts as the insulating inner wall of the thruster.

Four ring shaped sets of samarium-cobalt (SmCo) magnets are placed inside the inner quartz tube and in contact with the

outer ceramic wall. The inner magnetic circuit is 30 mm long and 20 mm in diameter. Two ferrite discs are placed on both extremities of the inductive coil, with SmCo magnets fixed around the ferrite discs, and a low-loss ferrite of 10 mm in diameter is set at the center of the cylinder. An L-shaped soft iron piece links the two outer rings of SmCo. This magnetic circuit allows generating the magnetic barrier in the exhaust plane (called first magnetic barrier) and the specific magnetic configuration in the ionization chamber and close to the anode. Four magnetic cusps with magnetic lines parallel to the walls lower particle losses and a second magnetic barrier (with magnetic field lines perpendicular to the electron current path) is located near the anode region. A zero-B field region appears in front of the inductive coil. The magnetization inside the magnetic barrier is oriented from the outer surface to the inner cylinder near the exhaust plane and inversely near the anode region. Hence, looking at the thruster from the exhaust side, the azimuthal $\mathbf{E} \times \mathbf{B}$ drift is clockwise oriented in the magnetic barrier on the cathode side, where the E field is oriented from anode to cathode, and clockwise or anticlockwise oriented near the anode, depending on the sign of the E field in this region.

Xenon flow Q_{Xe} is injected in the thruster through a Mullite ceramic. The discharge voltage U_d is applied between the anode and the cathode, and a starter tip near the cathode is used to ignite the plasma discharge. The anode consists of a copper disc of 40 mm diameter and 4 mm width segmented in 4 pieces electrically insulated, and is covered on the back side and on the inner and outer diameters by an insulating ceramic. The anode segments are mounted on an axial translator and are localized in this study at the maximum B field intensity of the second magnetic barrier (the distance from the exhaust plane is $z_{anode} = -31 \pm 0.5mm$ so that the surface of the disc is assumed to be parallel to the magnetic field lines, limiting electron short-circuit currents).

B. Triangulation method

The magnetic configuration and the geometry of the ID-Hall thruster (with a classic accelerator channel and a conical ionization chamber upstream) is appropriate to localize in 3D (in r, θ and z coordinates) the azimuthal instabilities in the kHz range. In order to be able to get an estimate of the axial position of these structures, a triangulation method based on parallax has been developed.

The parallax is the difference in the apparent position of an object viewed along two different lines of sight. Hence, from the observation of the position of an object along two lines of sight (e.g. two incidence angles) and knowing the distance between these two viewpoints, the distance separating the observer from the object can be inferred. This method is called triangulation method. In our case, the goal is therefore to be able to determine from the parallax, using the triangulation method, the axial position (z coordinate) of local instabilities versus time in the three main centimetric regions of the thruster presented in Fig. 2 and defined as follows: "near anode region", "0B region" and "channel region".

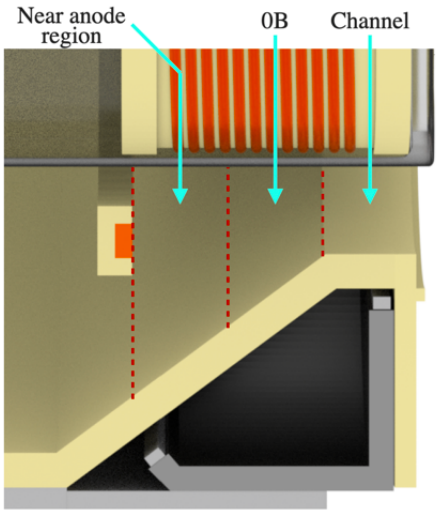

Figure 2. Representation of the three distinct zones as described in the text, "near anode region", "0B region" and "channel region".

1. *Apparatus*

In order to characterize these rotating structures, we used a FASTCAM Mini AX50/100 camera with 16-bit grey scale data coding, a 105 mm lens diameter with a 62 mm focal length. This camera can capture speeds of more than 500 000 fps (frames per second). However, the capture speed is strained by the size of the recording window. The larger the image size, the more pixels it will contain and the slower the capture speed will be, and vice versa. To meet our needs, we chose a recording window of 128x64 pixels and a maximum capture speed of 127 500 fps (time interval is therefore 7.8 μs). This capture speed allows us observing one structure moving at a maximum speed of 7250 m/s. For each experimental condition, 150 consecutive images are recorded corresponding to a total interval time of approximately 1.2 ms.

Previous high-speed camera investigations of azimuthal instabilities in single-stage thrusters have been performed without axial resolution.[8,20–22] In order to study these structures and to be able to compare our results with the literature, a first viewpoint was fixed in front of the thruster, e.g. on the thruster axis ($i_1 = 0°$) and the second one at $i_2 = 30°$ as shown in Fig. 3-a.

As for time resolved measurements the two images must be recorded simultaneously, a reflective mirror is positioned on each line of sight at three meters from the exhaust plane of the thruster in order to return both images on a 90° prism in front of the camera. Due to the low signal to noise ratio, the relatively small number of pixels and the conical geometry of the ionization chamber, a numerical code was developed under $MATLAB^{@}$ (Matrix Laboratory) to extract the characteristics of the instability. The code is split into two main parts. The first part treats the front image and determines the speed, the rotation frequency, the angular velocity and the mode.[37] The second part uses the two viewpoints and the triangulation method to infer the size and the location of the instabilities in

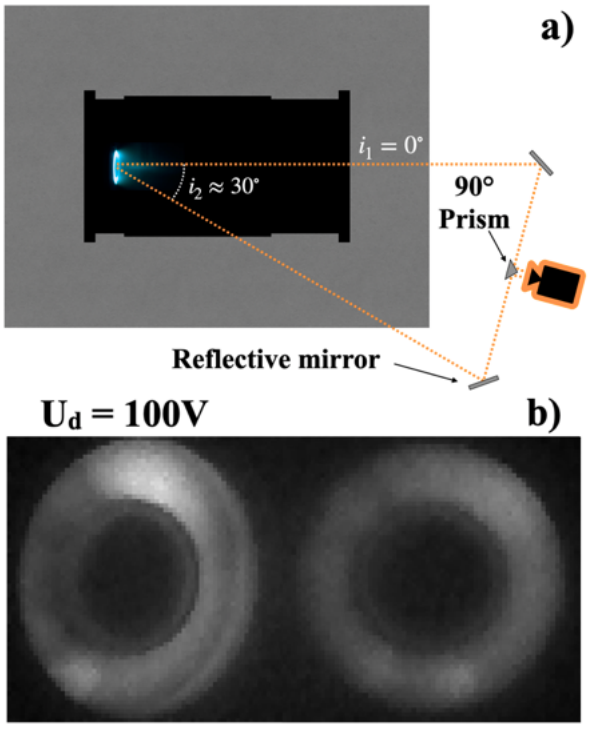

Figure 3. a- Schematic representation of the experimental device (top view) showing the chamber, the thruster, the optical elements, the camera and the optical paths (dot lines), b- Example of images recorded by the camera ($U_d = 100\,V$, $Q_{Xe} = 6\,sccm$). The image on the right corresponds to the front view and the image on the left to the view at $i_2 = 30°$.

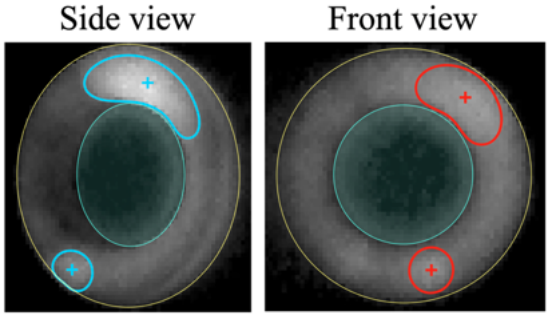

Figure 4. Highlighting two spokes on the side view (in blue) and the front view (in red) as well as the contours of the thruster.

$r - \theta - z$ as a function of time.

2. *Determination of the axial position of azimuthal instabilities*

In order to present the triangulation method in the context of spoke location in a Hall thruster, we will consider the experimental condition of Fig. 3-b. Fig. 4, representing the two view point images, highlights two local plasma brightness

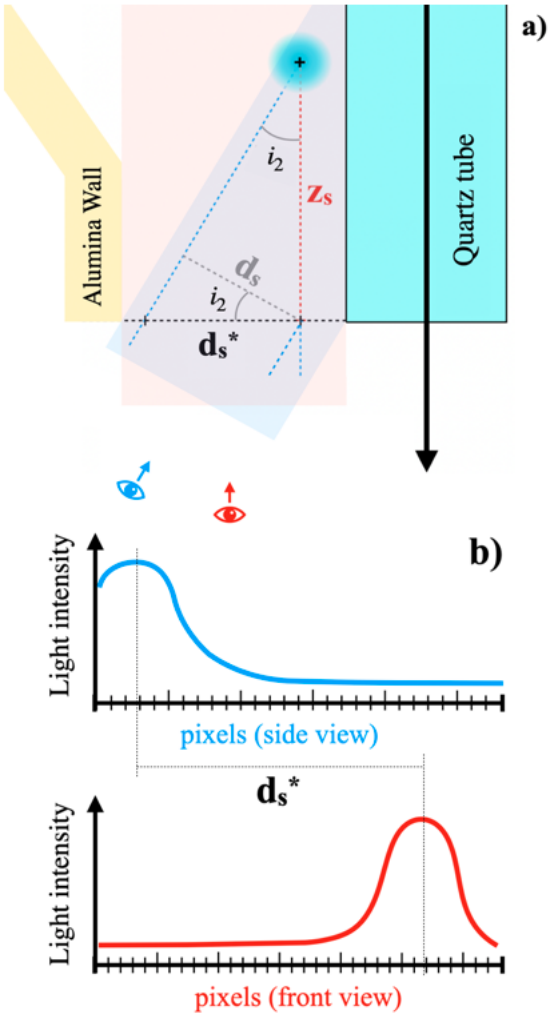

Figure 5. a- Schematic representation of a cross section of the ID-Hall thruster in the observation plane (horizontal) and of the different characteristic lengths to be determined for the use of triangulation method. Spoke position is artificially represented by the black + symbol. b- Schematic representation of the light intensities along the section according to the two viewpoints (blue on the side view, and red on the front view).

maxima corresponding to two azimuthal instabilities. These maxima are surrounded and centered by "+" symbols. The thruster exhaust plane is also represented by the outer wall of the channel in yellow and the inner wall in cyan. These images illustrate the parallax effect with the difference of the apparent positions of the same objects viewed along two lines of sight. With measuring the difference in position, we can infer an estimate of the axial position of the instabilities inside the thruster. Due to the conical geometry of the thruster and experimental constraints with shading effects (due to the opaque walls of the thruster), some assumptions have to be made (see Fig. 5-a):

- The two reflecting walls (mirrors and prism) and the transparent elements (windows of the vessel and various

optical lenses in the camera) between the plasma and the camera have a negligible geometric aberration and light absorption.

- The optical paths are horizontal and in the same plane.
- Relative to the size of the thruster, the images are recorded at a sufficiently large distance (3 m) to consider an orthographic projection and therefore a negligible perspective effect (the vanishing point is considered to be at infinity).
- The position of the azimuthal instabilities is bounded laterally by the walls of the thruster and axially by the anode and the exhaust plane.
- The plasma is considered to be optically thin: photons emitted by the plasma are not reabsorbed by the plasma.
- Plasma instabilities are considered to be spherical: the maximum of luminosity will be considered as the position of the instability.

From these assumptions, the axial position of an instability is obtained by determining the distance d_s^* separating each maximum of light intensity. Fig. 5-b represents the light intensity along the azimuthal direction for both viewpoints, from which d_s^* is obtained. Note that for simplicity in processing the images, the side view ($i_2 = 30°$) is stretched by a factor of $1/\cos(i_2)$. This increases the real distance d_s between the maxima that is inferred from the formula $d_s = d_s^*.cos(i_2)$.

To apply this method to the case of Fig. 4, a first treatment of the front and side images is performed. In order to clearly obtain the luminous intensity of the azimuthal instabilities, the time integrated luminosity of the plasma (time average of the 150 images in the sequence) is subtracted for each image. Then, for a pixel of (x,y) coordinates of an image i and for a viewpoint v, the variable part of the instantaneous luminosity $L^*_{S_{i,v}}(x,y)$ is expressed as follows:

$$L^*_{S_{i,v}}(x,y) = \frac{L_{S_{i,v}}(x,y)}{< L_{S_{i,v}}(x,y) >_{(x,y)}} - \frac{< L_{S_{150i,v}}(x,y) >_t}{<< L_{S_{150i,v}}(x,y) >_t >_{(x,y)}}$$

$L_{S_{i,v}}(x,y)$ corresponds to the light intensity of an image i contained in the (x,y) pixel. This value is normalized by the spatial average of the light intensity $< L_{S_{i,v}}(x,y) >_{(x,y)}$. $< L_{S_{150i,v}}(x,y) >_t$ is the temporal average of the 150 image sequence and $<< L_{S_{150i,v}}(x,y) >_t >_{(x,y)}$ its spatial average. Using this processing, we obtain the variable luminosity of the plasma pointing out the instabilities. Note that this operation minimizes the constant reflection of the light emitted by the plasma on the alumina walls. Indeed, while the external alumina wall (white) is clearly visible on the side view (see Fig. 3-b), it becomes much less marked on the side view after treatment (see Fig. 6).

The position of the instabilities is determined as follows: (i) first, from the front view (Fig. 6-a), the coordinates r and θ and the size of the instabilities (symbolized by a black circle magenta point) are determined, (ii) second, from the

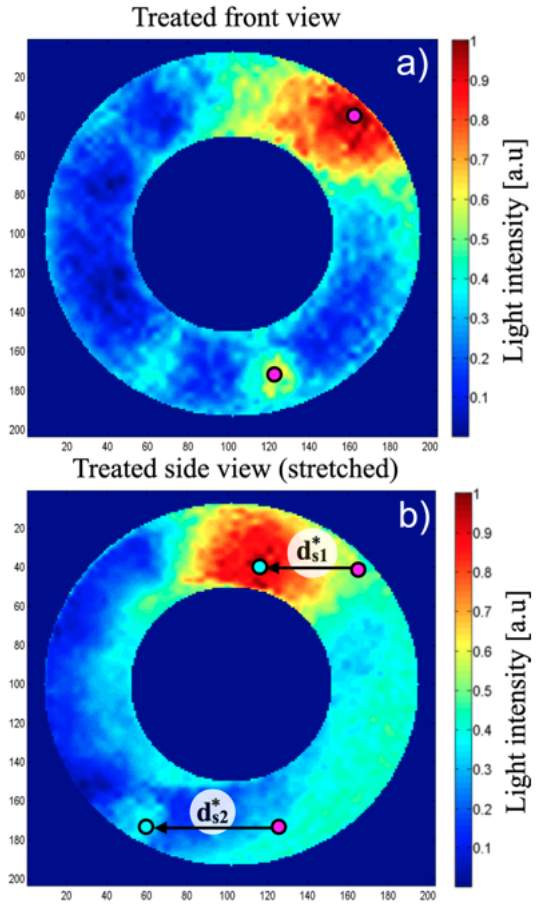

Figure 6. False-color representation of the varying brightness of the plasma. a) front view with two spokes. b) Stretched side view with two spokes and their respective distance d^*_{s1} and d^*_{s2}.

side viewpoint (Fig. 6-b), the distance d_s^* separating the closest maxima in the observation plane (horizontal) between the front view and the side view (black circle blue point) is determined. From the distance d_s^* for each instability, the depth z_s from the exhaust plane is deduced using the equation:

$$z_s = \frac{d_s^*.cos(i_2)}{sin(i_2)} = \frac{d_s^*}{tan(i_2)}$$

3. *Limitations of the triangulation method*

When the instabilities are localized close to the anode, the light emission from the rotating structure can be obstructed by the opaque walls of the thruster when performing image recording at $i_2 = 30°$. It is then not possible to estimate the axial position of the instability by the triangulation method. This limitation has been investigated using three laser pointers placed in front of the thruster to position three light points distributed azimuthally on the anode as depicted in Fig. 7-a. The anode can be moved axially between z=-12,5 mm and z=-52,5 mm from the exhaust plane. With knowing the exact

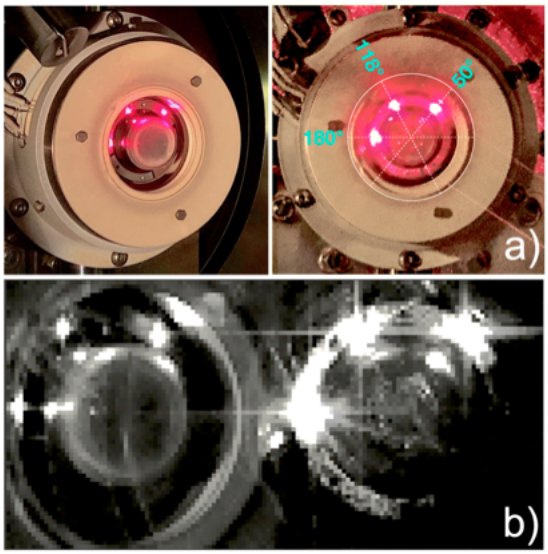

Figure 7. a- Front and side pictures of the reflection of the laser pointers. b- Image recorded by the high-speed camera in this configuration (anode position is $z_{anode} = -12.5\ mm$).

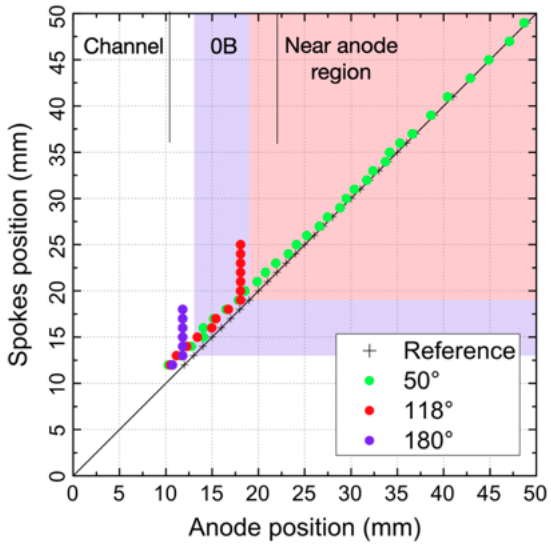

Figure 8. Representation of the axial position of the laser reflection obtained by the triangulation method as a function of the real position (position of the anode) for 3 different azimuthal positions (50°, 118° and 180°).

position of the anode, we can determine the obstruction limit by the walls and estimate the sensibility of the triangulation method in determining the position of the laser point.

Fig. 8 shows the evolution of the position of the laser points determined by the triangulation method as a function of the anode position. For the light spot at 50° (see Fig. 7-b) the position determined by the method is very close to the anode position demonstrating that the sensitivity of the method is high enough to distinguish the location of an instability in the three main centimetric regions described before. For the two other

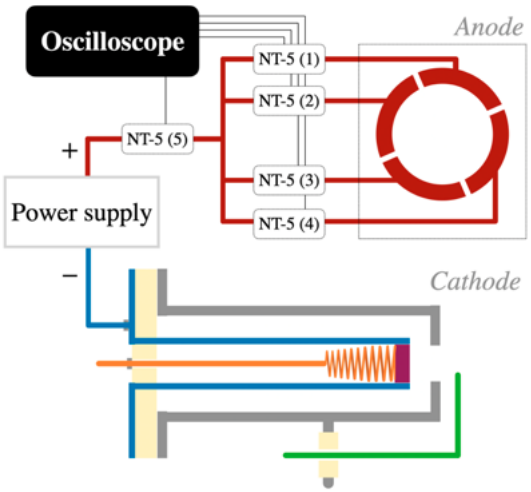

Figure 9. Schematic representation of the current measuring system using the segmented anode.

spots, the limitation of the technique is due to the presence of the opaque walls and can be clearly identified (13 mm at 180° and 19 mm at 118° from the exhaust plane). Hence, the axial position of an instability azimuthally located at 180° can be determined only if this instability is in the channel region.

C. Segmented anode

In order to complement the observations with the high-speed camera, a segmented anode was also used to record the electrical signature of the instabilities.[20,22] This anode is a flat stainless-steel ring with inner and outer diameters of 32 mm and 40 mm, respectively. The anode is segmented into 4 regular segments. Each segment is connected to the discharge power supply through a magneto-resistive current sensor. The total discharge current I_d is measured through a fifth sensor placed between the 4 segments and the power supply, as shown in Fig. 9. This system allows following the temporal variations of the collected current with a spatial resolution in the azimuthal direction. The sensitivity of each sensor is better than 0.3% and their reaction time is less than 150 ns. A low frequency generator and two oscilloscopes (TDK 2004B) allow triggering and recording the measurements as well as synchronizing the current traces with the images from the camera.

III. RESULTS

In the following experiments, the anode is located in the second magnetic barrier region where the magnetic field intensity is maximum ($z_{anode} = -31$ mm). The anode flow rate is varied from 6 sccm to 9 sccm. The specific magnetic configuration of the ID-Hall thruster (cf. II.A) does not significantly alter the appearance and the development of the classical low frequency instabilities found in conventional Hall thruster, e.g.

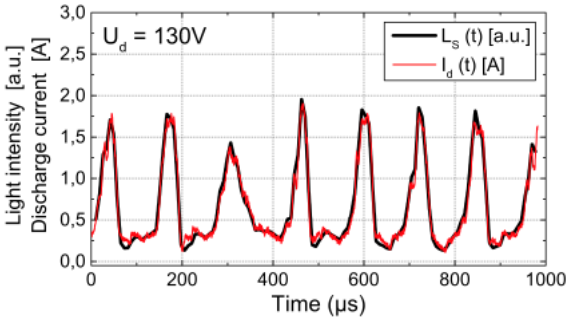

Figure 10. Discharge current $I_d(t)$ in red and light intensity $L_s(t)$ as a function of time for $U_d = 130\,V$.

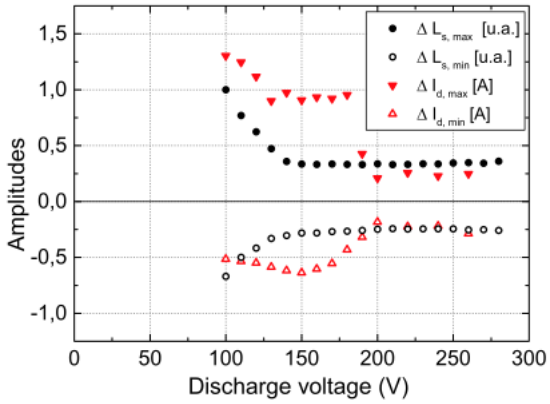

Figure 11. Average amplitudes of current oscillations (red triangles) and azimuthal variations of brightness (black points) as a function of the discharge voltage for 6 sccm xenon flow rate.

the breathing mode oscillations and the large-scale azimuthal instabilities.[36,37]

A. Breathing mode oscillations

Fig. 10 shows the discharge current $I_d(t)$ the integrated light intensity $L_s(t)$ versus time. For comparative purposes, the brightness of the plasma is normalized by its own average value and then multiplied by the average value of the discharge current. Under these conditions ($U_d = 130\,V$) the oscillation frequency is around 5.8 kHz. This instability corresponds to the breathing mode.[9,36] There is a clear correlation between light emission and the total discharge current. These results are in agreement with previous studies showing a strong correlation between luminosity and current related to an oscillation of electron-neutral collisions producing radiative deexcitations.[38–40]

B. Large-scale azimuthal instability

Depending on the discharge voltage applied between the anode and the cathode, azimuthal instabilities and/or the breathing mode can be observed. It is interesting to identify the range of appearance of both instabilities and quantify their importance versus the applied voltage using imaging characterization and current measurements. To identify the voltage range of rotating spoke appearance, the maximum L_{S,max_i}, the minimum L_{S,min_i} and average light intensities $< L_{S_i}(x,y) >_{(x,y)}$ are determined numerically. The average light intensity is then subtracted from the minimum and maximum intensities, such as:

$$\Delta L_{S,max_i} = L_{S,max_i} - < L_{S_i}(x,y) >_{(x,y)}$$

$$\Delta L_{S,min_i} = L_{S,min_i} - < L_{S_i}(x,y) >_{(x,y)}$$

These differences of brightness are then time averaged on the 150 images of each recorded sequence and for all explored conditions.

The strength of the breathing mode is determined from the amplitude of the discharge current by calculating the difference between the maximum $I_{d,max}$ (or minimum $I_{d,min}$) and the time average value $< I_d(t) >_t$ such as:

$$\Delta I_{d,max} = I_{d,max} - < I_d(t) >_t$$

$$\Delta I_{d,min} = I_{d,min} - < I_d(t) >_t$$

Fig. 11 shows in black the azimuthal variations of the normalized mean luminosity (corresponding to the intensity of the azimuthal instabilities) and in red the amplitude variations of the discharge current (corresponding to the presence of the breathing mode). We note that the breathing mode is intense between $100V < U_d < 180V$ and that the rotating spokes are visible in a narrower voltage range $100V < U_d < 140V$. Thus, in ID-Hall thruster, large-scale azimuthal structures cannot be observed independently of the breathing mode, as in most of previous experimental studies.[18,32,33]

Electrical measurements at low discharge voltage were also carried out using the segmented anode in order to characterize this coexistence of axial and azimthal instabilities. The following measurements were carried out in different operating conditions. The material of the outer wall is $BNSiO_2$ instead of Alumina and the single anode has been replaced by a segmented anode. The change of these two elements did not modify the azimuthal and axial behavior of these instabilities.

Fig. 12 shows 6 consecutive images recorded by the fast camera in front of the thruster (after image processing as defined in section II.B.2). The anode segments are depicted by the 4 arcs of different colors. The corresponding currents (with the same color code and noted with SW, NW, NE and SE) are shown versus time in Fig. 12-b. The magenta curve depicted in Fig. 12-c is the sum of the current collected by the 4 segments and is related to the total discharge current $I_d(t)$. The black curve corresponds to the total light intensity of the plasma $L_s(t)$. We observe in Fig. 12-a the azimuthal displacement of a plasma instability moving in the clockwise

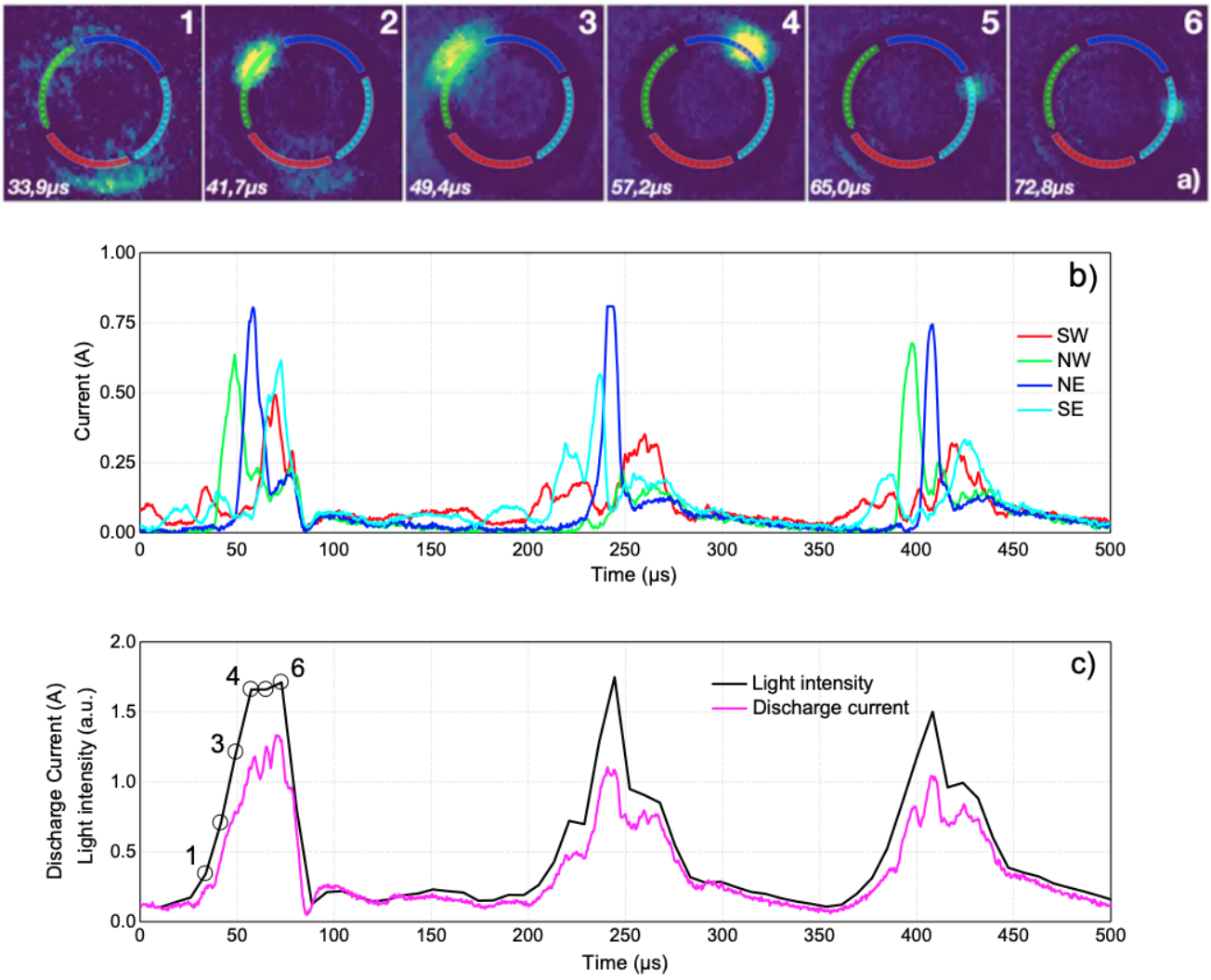

Figure 12. a- Successive images of the thruster from the front view after numerical processing showing only the variable brightness of the plasma (defined in section II.B.2). b- Temporal evolution of the current on each of the four segments of the anode. The corresponding currents are represented by the same color code than the one used in a- and are noted with SW, NW, NE and SE. c- Temporal evolution of the brightness of the plasma (in black) and of the total anode current. Discharge voltage is $U_d = 120V$. Xenon flow in the thruster is 6 sccm. Xenon flow rate in the cathode is 1.5 sccm.

direction. This is correlated with the fast increase of the discharge current or the integrated light emission in Fig. 12-c. The relative light emission of the spoke is intense during the current rise, and quickly decreases at the end of the current rise. Since the images are processed in such a way as to show the relative intensity of the spoke, this means that light emitted by the plasma tends to be more azimuthally uniform around the current maximum and current decay. We also see clearly the correlation between the azimutal position of the instability (strong light emission) and the evolution of the current on the four anode segments. We estimate from the measurements that $60 \pm 20\%$ of the discharge current flows through the rotating instability. This is similar to other studies estimating a discharge current collected on the anode in the region in front of the spoke at more than 50% of the value of the total current[20,22]. The fact that the total current is 60% of the discharge current does not mean that 60% of the ionization takes place in the spoke. As shown in Refs. [30,31] the presence of a spoke is associated with a deformation of the equipotential lines that creates a kind of short-circuit between acceleration region and anode. This deformation of the equipotential lines moves with the spoke. Note that the current measurements indicate that the rotating instability seems to propagate in the counterclockwise direction in some rare cases, like within the second current peak in Fig. 12-b around 250 μs. The reason for the apparently counterclockwise rotation around 250 μs is not clear. In a large majority of observations, the rotation was clockwise.

From the images in Fig. 12-a and the dimensions of the thruster given in section II-A, we estimate that the velocity of the rotating spoke is around 1800 $m.s^{-1}$. The $\mathbf{E} \times \mathbf{B}$ electron azimuthal drift velocity can be estimated from $u_{\mathbf{E}\times\mathbf{B}} = \frac{E}{B}$.

Taking $E = 10^4\ V.m^{-1}$ and $B = 0.02\ T$, it gives $u_{\mathbf{E}\times\mathbf{B}} = 5\times10^6\ m.s^{-1}$, much higher than the rotating spoke velocity.

C. Axial position of the azimuthal instability

Using the triangulation method, we were able to study the dynamics of instabilities under the conditions where rotating structures and breathing mode oscillations coexist. In order to clearly determine the position of the azimuthal instabilities in the axial direction, the anode flow rate was increased to $Q_{Xe} = 9sccm$ to enhance ionization and radiative emission of the plasma. Fig. 13 represents the axial position of the azimuthal instabilities in the thruster (blue circles) distributed between the exhaust plane of the thruster ($z = 0mm$) and the surface of the anode ($z_{anode} = -31mm$), as well as the total light emission of the plasma (in red) as a function of time, for $U_d = 100V$. We see that the axial position of the instabilities evolves over time and seems to be correlated with the evolution of the light intensity of the plasma $L_S(t)$, e.g. with the discharge current $I_d(t)$ (cf. III.A). The structures are present during the whole period of the breathing mode even during the quasi extinction of the discharge but are less visible during the current decay. During the increase of the light intensity (or discharge current), the structures are rotating azimuthaly in the clockwise direction (see Fig. 12) and are moving axially from the near-anode region to the channel region (in the direction of the ionization front of the breathing mode), describing an helicoidal motion. After reaching the maximum of the discharge current and during the light emission decay, the images exhibit a more azimuthally uniform luminous front moving from the channel exhaust to the chamber and anode region (this motion is indicated by the black arrows in Fig. 13) . After the current decay, the structures are located and are rotating in the near anode-region and stays in this region up to another cycle of the breathing mode. It has been recently suggested from fast camera analysis using POD method that rotating spokes (located in the near-anode region and with a mode m=1) and gradient driven instabilities (with modes higher than 1) might be present with the breathing mode oscillations[32].

IV. CONCLUSION

We have developed a non-perturbative triangulation method based on parallax that allows the 3D tracking of rotating spokes in a Hall thruster with a high-speed camera. This triangultion method has proved to be sufficiently sensitive to detect non-uniformities with a space resolution of a few millimeters. The triangulation method has been used to characterize the low frequency instabilities occuring in a double-stage thruster, ID-Hall, operating in a single stage mode, and has been coupled to current measurements on a segmented anode.

The measurements in the ID-Hall thruster show a strong correlation between axial oscillations of the ionization front in the breathing mode and azimuthal spoke rotation. In the conditions considered in this article, the spoke motion is helicoidal during the current rise, i.e. the spoke moves from the anode region toward the channel exhaust region while rotating in the $\mathbf{E}\times\mathbf{B}$ and seems to follow the movement of the front of neutral atoms progressively filling the channel. Around the maximum current and light emission intensity of the breathing mode the light emission appears to be more azimuthally uniform. During the current decay, the maximum luminosity of the plasma moves from the exhaust region to the chamber and anode without clear evidence of important azimuthal non-uniformity and azimuthal motion. This motion is most likely associated with the neutral atom depletion and motion of the ionization front inward. The high-speed camera also detects the presence of a smaller and less luminous region rotating in the $\mathbf{E}\times\mathbf{B}$ direction near the anode, even during the low current phase of the low frequency oscillations. This could be due to the specific magnetic configuration of ID-Hall, which presents a second magnetic barrier in front of the anode, leading to the formation of a rotating anode spot. Finally we note that low frequency oscillations can exist without the presence of rotating spokes. This is the so-called "global mode" of oscillations described by Sekerak et al.[8]) in a 6 kW Hall thruster. These authors also show the existence of a "local mode" of oscillations (obtained at higher magnetic field strengths) where spokes coexist with low amplitude current oscillations. The characteristics of these different modes certainly depend on the design and power of a specific Hall thruster. In the conditions considered in the present paper both large amplitude current oscillations and rotating spokes coexist and are correlated.

ACKNOWLEDGMENTS

This work is supported by CNES, the French Space Agency, and by the RTRA STAE foundation under the project INNPULSE.

REFERENCES

[1]J.-P. Boeuf, "Tutorial: Physics and modeling of hall thrusters," Journal of Applied Physics **121**, 011101 (2017).
[2]I. D. Kaganovich, A. Smolyakov, Y. Raitses, E. Ahedo, I. G. Mikellides, B. Jorns, F. Taccogna, R. Gueroult, S. Tsikata, A. Bourdon, J.-P. Boeuf, M. Keidar, A. T. Powis, M. Merino, M. Cappelli, K. Hara, J. A. Carlsson, N. J. Fisch, P. Chabert, I. Schweigert, T. Lafleur, K. Matyash, A. V. Khrabrov, R. W. Boswell, and A. Fruchtman, "Physics of exb discharges relevant to plasma propulsion and similar technologies," Physics of Plasmas **27**, 120601 (2020), https://doi.org/10.1063/5.0010135.
[3]A. Morozov, "The conceptual development of stationary plasma thrusters," Plasma Phys. Rep. **29**, 235 (2003).
[4]S. Mazouffre, "Electric propulsion for satellites and spacecraft: established technologies and novel approaches," Plasma Sources Science and Technology **25**, 033002 (2016).
[5]A. I. Morozov, Y. V. Esinchuk, and G. N. Tilinin, "Plasma accelerator with closed electron drift and extended acceleration zone," Sov. Phys.-Tech. Phys. **17**, 38–45 (1972).
[6]G. S. Janes and R. S. Lowder, "Anomalous electron diffusion and ion acceleration in a low-density plasma," The Physics of Fluids **9**, 1115–1123 (1966).
[7]E. Chesta, C. M. Lam, N. B. Meezan, D. P. Schmidt, and M. A. Cappelli, "A characterization of plasma fluctuations within a hall discharge," IEEE Transactions on Plasma Science **29**, 582–591 (2001).

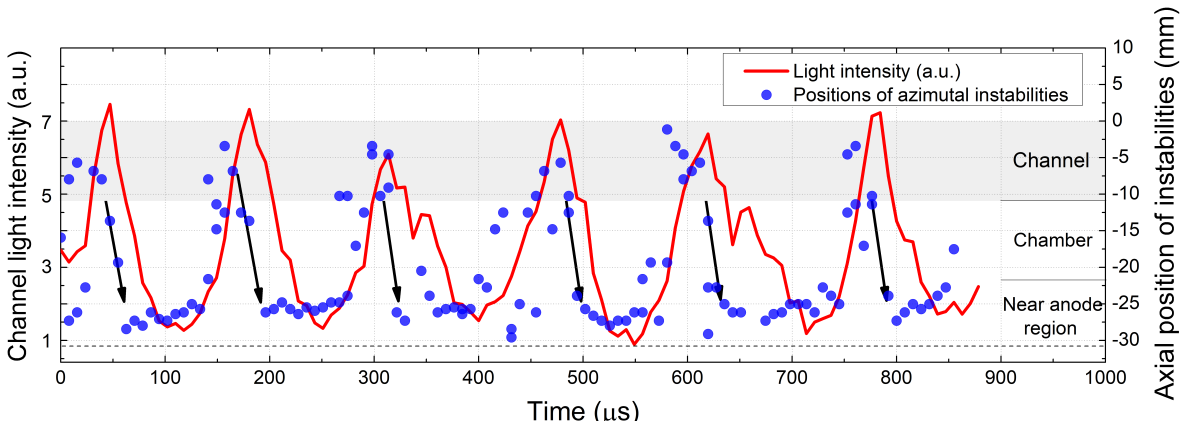

Figure 13. Axial position of azimuthal instabilities (blue circles) as a function of time. The red line represents the total light intensity of the channel versus time. The black arrows indicate schematically the motion of the ionization front from the exhaust plane to the chamber. The axial position of the exhaust plane and anode are 0 and - 31 mm respectively. The channel is represented by the greyed area and and the anode by the dashed line. Discharge voltage $U_d = 100V$, Xenon flow in the thruster $Q_{Xe} = 9sccm$ and Xenon flow rate in the cathode $Q_{Xe} = 1.5sccm$.

[8] M. J. Sekerak, A. D. Gallimore, D. L. Brown, R. R. Hofer, and J. E. Polk, "Mode transitions in hall-effect thrusters induced by variable magnetic field strength," Journal of Propulsion and Power **32**, 903–917 (2016).

[9] J. P. Boeuf and L. Garrigues, "Low frequency oscillations in a stationary plasma thruster," Journal of Applied Physics **84**, 3541–3554 (1998).

[10] J. Fife, M. Martinez-Sanchez, J. Szabo, J. Fife, M. Martinez-Sanchez, and J. Szabo, "A numerical study of low-frequency discharge oscillations in hall thrusters," in *33rd Joint Propulsion Conference and Exhibit*.

[11] S. Barral and E. Ahedo, "On the origin of low frequency oscillations in hall thrusters," AIP Conference Proceedings **993**, 439–442 (2008).

[12] T. Lafleur, R. Martorelli, P. Chabert, and A. Bourdon, "Anomalous electron transport in hall-effect thrusters: Comparison between quasi-linear kinetic theory and particle-in-cell simulations," Physics of Plasmas **25**, 061202 (2018).

[13] E. T. Dale and B. A. Jorns, eds., *Proceedings of the 36th International Electric Propulsion Conference* (2019) paper IEPC-2019-354.

[14] E. T. Dale and B. A. Jorns, eds., *Proceedings of the 36th International Electric Propulsion Conference* (2019) paper IEPC-2019-352.

[15] T. Lafleur, P. Chabert, and A. Bourdon, "The origin of the breathing mode in hall thrusters and its stabilization," Journal of Applied Physics **130**, 053305 (2021).

[16] O. Chapurin, A. Smolyakov, G. J. M. Hagelaar, J. P. Boeuf, and Y. Raitses, "Fluid and hybrid simulations of the ionization instabilities in hall thruster," (2022).

[17] K. Hara, M. J. Sekerak, I. D. Boyd, and A. D. Gallimore, "Perturbation analysis of ionization oscillations in hall effect thrusters," Physics of Plasmas **21**, 122103 (2014).

[18] Y. B. Esipchuk, A. I. Morozov, G. N. Tilinin, and A. V. Trofimov, "Plasma oscillations in closed-drift accelerators with an extended acceleration zone," Soviet Physics Technical Physics **18**, 928 (1973).

[19] J. B. Parker, Y. Raitses, and N. J. Fisch, "Transition in electron transport in a cylindrical hall thruster," Applied Physics Letters **97**, 091501 (2010).

[20] M. S. McDonald and A. D. Gallimore, eds., *Proceedings of the 32nd International Electric Propulsion Conference* (2011) paper IEPC-2011-242.

[21] S. Mazouffre, L. Grimaud, S. Tsikata, K. Matyash, and R. Schneider, "Rotating spoke instabilities in a wall-less hall thruster: experiments," Plasma Sources Science and Technology **28**, 054002 (2019).

[22] C. L. Ellison, Y. Raitses, and N. J. Fisch, "Cross-field electron transport induced by a rotating spoke in a cylindrical hall thruster," Physics of Plasmas **19**, 013503 (2012).

[23] J. Adam, A. Heron, and G. Laval, "Study of stationary plasma thrusters using two-dimensional fully kinetic simulations," Physics of Plasmas **11**, 295–305 (2004).

[24] J. P. Boeuf and L. Garrigues, "$\mathbf{E} \times \mathbf{B}$ electron drift instability in hall thrusters: Particle-in-cell simulations vs. theory," Physics of Plasmas **25**, 061204 (2018).

[25] A. Smolyakov, T. Zintel, L. Couedel, D. Sydorenko, A. Umnov, E. Sorokina, and N. Marusov, "Anomalous electron transport in one-dimensional electron cyclotron drift turbulence," Plasma Physics Reports **46**, 496–505 (2020).

[26] S. Tsikata, C. Honore, N. Lemoine, and D. M. Gresillon, "Three-dimensional structure of electron density fluctuations in the hall thruster plasma: Exb mode," Physics of Plasmas **17**, 112110 (2010), https://doi.org/10.1063/1.3499350.

[27] A. I. Smolyakov, O. Chapurin, W. Frias, O. Koshkarov, I. Romadanov, T. Tang, M. Umansky, Y. Raitses, I. D. Kaganovich, and V. P. Lakhin, "Fluid theory and simulations of instabilities, turbulent transport and coherent structures in partially-magnetized plasmas of $\mathbf{E} \times \mathbf{B}$ discharges," Plasma Physics and Controlled Fusion **59**, 014041 (2016).

[28] M. Panjan and A. Anders, "Plasma potential of a moving ionization zone in dc magnetron sputtering," Journal of Applied Physics **121**, 063302 (2017).

[29] A. Hecimovic and A. von Keudell, "Spokes in high power impulse magnetron sputtering plasmas," Journal of Physics D: Applied Physics **51**, 453001 (2018).

[30] J.-P. Boeuf and M. Takahashi, "Rotating spokes, ionization instability, and electron vortices in partially magnetized exb plasmas," Phys. Rev. Lett. **124**, 185005 (2020).

[31] J. P. Boeuf and M. Takahashi, "New insights into the physics of rotating spokes in partially magnetized exb plasmas," Physics of Plasmas **27**, 083520 (2020).

[32] V. Désangles, S. Shcherbanev, T. Charoy, N. Clément, C. Deltel, P. Richard, S. Vincent, P. Chabert, and A. Bourdon, "Fast camera analysis of plasma instabilities in hall effect thrusters using a pod method under different operating regimes," Atmosphere **11** (2020).

[33] I. Romadanov, Y. Raitses, and A. Smolyakov, "Hall thruster operation with externally driven breathing mode oscillations," Plasma Sources Sci. Technol. **27**, 09006 (2018).

[34] L. Dubois, F. Gaboriau, L. Liard, D. Harribey, C. Henaux, L. Garrigues, G. J. H. Hagelaar, S. Mazouffre, C. Boniface, and J. P. Boeuf, "Id-hall, a new double stage hall thruster design. i. principle and hybrid model of id-hall," Physics of Plasmas **25**, 093503 (2018).

[35] L. Dubois, F. Gaboriau, L. Liard, C. Boniface, and J. P. Boeuf, "Id-hall, a new double stage hall thruster design. ii. experimental characterization of the inductive ionization source," Physics of Plasmas **25**, 093504 (2018).

[36] A. Martín Ortega, A. Guglielmi, F. Gaboriau, C. Boniface, and J. P. Boeuf, "Experimental characterization of id-hall, a double stage hall thruster with an inductive ionization stage," Physics of Plasmas **27**, 023518 (2020).

[37] A. Guglielmi, A. Martin Ortega, F. Gaboriau, and J. Boeuf, eds., *Proceedings of the 36th International Electric Propulsion Conference* (2019) paper IEPC-2019-632.

[38] R. Lobbia, T. Liu, and A. Gallimore, "Temporally and spatially resolved measurements in the plume of clustered hall thrusters," 45th

AIAA/ASME/SAE/ASEE Joint Propulsion Conference and Exhibit (2009), 10.2514/6.2009-5354.

[39]K. Hara, M. J. Sekerak, I. D. Boyd, and A. D. Gallimore, "Mode transition of a hall thruster discharge plasma," Journal of Applied Physics **115**, 203304 (2014).

[40]M. J. Sekerak, R. R. Hofer, J. E. Polk, B. W. Longmier, A. Gallimore, and D. L. Brown, "Mode transitions in hall effect thrusters," in *49th AIAA/ASME/SAE/ASEE Joint Propulsion Conference*.